Seikichi Matsuoka, Shinsuke Satake, Masayuki Yokoyama, Arimitsu Wakasa, and Sadayoshi Murakami

Related Articles

Additional information on Phys. Plasmas

Journal Homepage: http://pop.aip.org/

Journal Information: http://pop.aip.org/about/about_the_journal

Top downloads: http://pop.aip.org/features/most_downloaded

Information for Authors: http://pop.aip.org/authors

Neoclassical electron transport calculation by using δf Monte Carlo method

Seikichi Matsuoka,[1,a] Shinsuke Satake,[1,2] Masayuki Yokoyama,[1,2] Arimitsu Wakasa,[3] and Sadayoshi Murakami[3]

[1]*The Graduate University for Advanced Studies (SOKENDAI), Toki 509-5292, Japan*
[2]*National Institute for Fusion Science, Toki 509–5292, Japan*
[3]*Department of Nuclear Engineering, Kyoto University, Kyoto 606–8501, Japan*

High electron temperature plasmas with steep temperature gradient in the core are obtained in recent experiments in the Large Helical Device [A. Komori *et al.*, Fusion Sci. Technol. **58**, 1 (2010)]. Such plasmas are called core electron-root confinement (CERC) and have attracted much attention. In typical CERC plasmas, the radial electric field shows a transition phenomenon from a small negative value (ion root) to a large positive value (electron root) and the radial electric field in helical plasmas are determined dominantly by the ambipolar condition of neoclassical particle flux. To investigate such plasmas' neoclassical transport precisely, the numerical neoclassical transport code, FORTEC-3D [S. Satake *et al.*, J. Plasma Fusion Res. **1**, 002 (2006)], which solves drift kinetic equation based on δf Monte Carlo method and has been applied for ion species so far, is extended to treat electron neoclassical transport. To check the validity of our new FORTEC-3D code, benchmark calculations are carried out with GSRAKE [C. D. Beidler *et al.*, Plasma Phys. Controlled Fusion **43**, 1131 (2001)] and DCOM/NNW [A. Wakasa *et al.*, Jpn. J. Appl. Phys. **46**, 1157 (2007)] codes which calculate neoclassical transport using certain approximations. The benchmark calculation shows a good agreement among FORTEC-3D, GSRAKE and DCOM/NNW codes for a low temperature ($T_e(0) = 1.0$ keV) plasma. It is also confirmed that finite orbit width effect included in FORTEC-3D affects little neoclassical transport even for the low collisionality plasma if the plasma is at the low temperature. However, for a higher temperature (5 keV at the core) plasma, significant difference arises among FORTEC-3D, GSRAKE, and DCOM/NNW. These results show an importance to evaluate electron neoclassical transport by solving the kinetic equation rigorously including effect of finite radial drift for high electron temperature plasmas. © *2011 American Institute of Physics*. [doi:10.1063/1.3562890]

I. INTRODUCTION

Collisional diffusion of neoclassical (NC) transport has attracted much attention recently to improve the confinement property in helical devices such as the large helical device (LHD), since NC transport causes an inevitable level of particle and energy diffusion in torus plasmas and this NC diffusion coefficient increases in proportion to $T_{e,i}^{7/2}$ in the $1/\nu_{e,i}$ regime in three-dimensional magnetic configurations in helical devices, where $T_{e,i}$ is the temperature and $\nu_{e,i}$ is the collision frequency of electron or ion species. Therefore, it is of great importance to evaluate the NC diffusion coefficient for high T_e plasmas accurately in helical devices. In LHD, high electron temperature plasmas [$(T_e \simeq 15$ keV) (Ref. 1)] have been obtained in recent experiments. Such plasmas, are called core electron-root confinement (CERC),[2] since these plasmas have a strong positive radial electric field called electron root, and CERC plasmas also have the steep T_e gradient called electron internal transport barrier (eITB). Moreover, the radial electric field (E_r) shows a transition phenomenon from a small negative value (ion root) to an electron root when eITB and then CERC plasma is formed.[3,4] Furthermore, E_r in helical plasmas is determined dominantly by the NC ambipolar condition,[5] which is the balance relation on E_r between electron and ion particle flux, that is, $\Gamma_e(E_r) = \Gamma_i(E_r)$, where Γ_a is the particle flux of species a. Experimental radial transport level is in general much larger than that obtained by NC theory due to anomalous or turbulence transport. It was shown in the recent studies that the anomalous transport is reduced by the E_r shear (Ref. 6 for example), while the reduction of the NC transport is determined by E_r itself and its direction, or the sign of E_r. The exact evaluation of NC transport particle and/or energy flux including FOW effect in such high electron temperature plasmas like CERC has a significant importance to clarify the behavior of the ambipolar radial electric field that reduces transport levels in the plasma core.

So far, NC transport calculations for electrons have been conventionally carried out assuming that electrons are located at a certain local magnetic surface, that is, the radial drift width of particle orbit is neglected (it is so called local or conventional treatment), for example, by GSRAKE[7,8] and DCOM/NNW[9,10] code. However, it has been pointed out in Ref. 11 that nonlocal contributions to NC transport needs to be retained in asymmetric devices where the large deviations of the particles from their initial magnetic surfaces may appear.

The finite orbit width (FOW) effect or the width of the electron drift in helical systems for a case of $E_r=0$ is roughly estimated by Δ_h as follows:[12]

a)Electronic mail: matsuoka.seikichi@LHD.nifs.ac.jp.

$$\Delta_{\mathrm{h}} = \frac{V_\perp}{\nu_{\mathrm{eff}}} \simeq \frac{\epsilon_{\mathrm{h}}}{\nu_{\mathrm{ei}}} \frac{T_{\mathrm{e}}}{eBR}, \tag{1}$$

where $V_\perp$ denotes the typical drift velocity of the guiding center, ν_{eff} is effective collisionality, ϵ_{h} is the helicity in the magnetic field, R is the major radius, and ν_{ei} is the electron-ion collision frequency. When the radial electric field exists, the drift width of a trapped particle is estimated according to Ref. 12 as follows,

$$\Delta_{\mathrm{h}} = \frac{V_\perp}{\omega_{E \times B}} \simeq \epsilon_{\mathrm{t}} \frac{T_{\mathrm{e}}}{eE_{\mathrm{r}}}, \tag{2}$$

where $\omega_{E \times B}$ denotes the poloidal precession frequency by the $E \times B$ drift, $\epsilon_{\mathrm{t}} = r/R$ is the toroidicity of the magnetic field and r is the minor radius. Since the drift width of a helical trapped particle, Δ_{h}, increases either as $\Delta_{\mathrm{h}} \propto T_{\mathrm{e}}/\nu_{\mathrm{ei}}$ for the case of $E_{\mathrm{r}} = 0$ or as $\Delta_{\mathrm{h}} \propto T_{\mathrm{e}}$ for the case with E_{r}, it is uncertain whether the conventional neoclassical transport theory is rigorously valid for CERC plasmas because of its high T_{e}. It is noted that the steep temperature gradient may also affect the NC transport property when concerning CERC plasmas.

To investigate the finite orbit width effects on NC transport in high T_{e} plasma, FORTEC-3D code,[13,14] which numerically solves the drift kinetic equation including the FOW effect of particles in three-dimensional magnetic configurations based on δf Monte Carlo method,[15,16] is extended for electron NC calculations. Since finite radial drift of a particle is included in FORTEC-3D, it can calculate NC transport nonlocally with less approximation than other codes based on local NC transport theory. It is noticed that all constants of motion such as total particle number, momentum, and energy are conserved by this collision term for like-particle collisions.

The remainder of this paper is organized as follows. In Sec. II, δf Monte Carlo method to solve the drift kinetic equation is reviewed briefly. A new electron-ion collision term, which is implemented in FORTEC-3D, is also described. Brief review for the difference between FORTEC-3D, GSRAKE, and DCOM/NNW codes is also given. Then, FORTEC-3D are applied for a low temperature plasma and the total mode number dependence of magnetic field for FORTEC-3D simulation is investigated in Sec. III. Benchmark calculations among FORTEC-3D, GSRAKE, and DCOM/NNW are also presented. In Sec. IV, NC transport flux is calculated for two cases both in low collisionality regime: (1) a plasma with low temperature and low density and (2) a plasma with high temperature. These two cases have similar collisionalities, however, it is shown that flux dependence on E_{r} differs from each other. Summary and discussion are given in Sec. V.

II. NUMERICAL METHOD

A. δf Monte Carlo method

In this section, δf Monte Carlo method are briefly reviewed, then, modification for FORTEC-3D[14] to treat electron NC transport are explained. δf Monte Carlo method are widely used to solve drift kinetic (DK) equation and gyroki-

netic equation in recent research. In FORTEC-3D, to be applicable to general three-dimensional magnetic configurations, Boozer coordinates[17] are adopted, and DK equation for a-th species distribution function $f_{\mathrm{a}}(\boldsymbol{R}, K, \mu; t)$ are described in $(\boldsymbol{R}, K, \mu; t)$ coordinates,

$$\frac{\partial f_{\mathrm{a}}}{\partial t} + \dot{\boldsymbol{R}} \cdot \nabla f_{\mathrm{a}} + \dot{K} \frac{\partial f_{\mathrm{a}}}{\partial K} = C_{\mathrm{a}}(f_{\mathrm{a}}), \tag{3}$$

where $\boldsymbol{R}$ is the guiding center position vector in Boozer coordinates (Ψ, θ, ζ), and K and μ are the kinetic energy and the magnetic moment, respectively. It is noted that Ψ, θ, ζ represent the toroidal magnetic flux, the poloidal angle, and the toroidal angle, respectively, and magnetic field $\boldsymbol{B}$ is represented as $\boldsymbol{B} = \nabla \Psi \times \nabla \theta + \iota \nabla \zeta \times \nabla \Psi$ in this coordinate. The strength of the magnetic field in Boozer coordinates can be represented by the sum of its Fourier components as follows,

$$B(\Psi, \theta, \zeta) = \sum_{m,n} B(\Psi)_{mn} \cos(m\theta - n\zeta), \tag{4}$$

where m, n are the poloidal and the toroidal mode number, respectively. The guiding center equation of motion in Boozer coordinates are given as a Hamiltonian formulation in the Ref. 18 and 19. It is also noted that both parts of distribution function are independent of gyroangle variable, since in DK equation, only gyroindependent part can be treated. Linearized collision term $C_{\mathrm{a}}(f_{\mathrm{a}})$ is defined as $C_{\mathrm{a}}(f_{\mathrm{a}}) \equiv \Sigma_{\mathrm{b}} C_{\mathrm{a,b}}[f_{\mathrm{a}}, f_{\mathrm{b}}]$. $\dot{\boldsymbol{R}}$ and $\dot{K}$ are written as following equations,

$$\dot{\boldsymbol{R}} = \boldsymbol{v}_\parallel + \boldsymbol{v}_{\mathrm{d}} \tag{5}$$

$$\dot{K} = e_{\mathrm{a}} \boldsymbol{v}_{\mathrm{d}} \cdot \boldsymbol{E}_{\mathrm{r}}, \tag{6}$$

where, $v_\parallel = \dot{\boldsymbol{R}} \cdot \boldsymbol{b}$ and $\boldsymbol{v}_{\mathrm{d}}$ is the drift velocity of the guiding center perpendicular to the magnetic field composed of $E \times B$, ∇B, and the curvature drift, and $\boldsymbol{b}$ is a unit vector tangential to magnetic field $\boldsymbol{B}$. E_{r} represents the radial electric field, where potential Φ is assumed to depend only on the flux surface label Ψ. Particle distribution function is separated into two parts,

$$f_{\mathrm{a}} = f_{M,\mathrm{a}}(\Psi, v) + \delta f_{\mathrm{a}}(\boldsymbol{R}, K, \mu, t), \tag{7}$$

where $f_{M,\mathrm{a}}$ represents the local Maxwellian distribution defined as $f_{M,\mathrm{a}} = n_{\mathrm{a}}(m/2\pi T_{\mathrm{a}})^{3/2} \exp[-(K/T_{\mathrm{a}})]$ and δf_{a} is a deviation from $f_{M,\mathrm{a}}$ in total distribution function f_{a}. Furthermore, Eq. (3) is rewritten for the first order as follows:

$$\frac{D\delta f_{\mathrm{a}}}{Dt} = -\left(\boldsymbol{v}_{\mathrm{d}} \cdot \nabla + \dot{K} \frac{\partial}{\partial K} \right) f_{M,\mathrm{a}} + C_{\mathrm{FP}}(f_{M,\mathrm{a}}). \tag{8}$$

It is noted that the operator D/Dt is defined by following equation

$$\frac{D}{Dt} \equiv \frac{\partial}{\partial t} + (\boldsymbol{v}_\parallel + \boldsymbol{v}_{\mathrm{d}}) \cdot \nabla + \dot{K} \frac{\partial}{\partial K} - C_{\mathrm{TP}}, \tag{9}$$

and denotes a time derivative along a particle trajectory,[20] where C_{TP} and C_{FP} is test particle and field particle part of the linearized collision operator C_{a}. In δf Monte Carlo method, DK Eq. (8) for the first order distribution function

δf is solved by following orbit trajectories of a large number of marker particles with proper collision operator. In FORTEC-3D, two kinds of weight, w_i and p_i for each marker particle are introduced according to the two weight scheme adopted in the Refs. 15 and 16, where subscript i denotes marker particle number. Time evolution for w_i and p_i are described as following equations,

$$\dot{w}_i = \frac{p_i}{f_{M,a}}\left(-\boldsymbol{v}_d \cdot \nabla - \dot{K}\frac{\partial}{\partial K} + C_{FP}\right)f_{M,a}, \qquad (10)$$

$$\dot{p}_i = \frac{p_i}{f_{M,a}}\left(\boldsymbol{v}_d \cdot \nabla + \dot{K}\frac{\partial}{\partial K}\right)f_{M,a}. \qquad (11)$$

Time evolution for each marker particle's variables, $(\boldsymbol{R}_i, K_i, \mu_i, w_i, p_i; t)$ are followed and then δf after several time steps are simulated numerically by summation of the whole marker particles, namely:

$$\delta f = \sum_i \frac{w_i}{J}\delta(\boldsymbol{R}-\boldsymbol{R}_i)\delta(K-K_i)\delta(\mu-\mu_i), \qquad (12)$$

where J denotes the Jacobian of the phase space $(\boldsymbol{R}, K, \mu)$. NC particle flux Γ_a and energy flux Q_a are given as follows:

$$\Gamma_a = \left\langle \int d^3v\,\dot{\Psi}\,\delta f \right\rangle, \qquad (13)$$

$$Q_a = \left\langle \int d^3v\,\frac{1}{2}m_a v^2 \dot{\Psi}\,\delta f \right\rangle, \qquad (14)$$

where $\langle\cdots\rangle$ denotes a flux surface average. It is noted that in FORTEC-3D calculations lost marker particles which remain out of the last closed flux surface at a particular time are killed and recycled inside the plasma domain. The weights of recycled marker particles are determined not to add any physical values such as the density, momentum, and energy to the rebirth point.[13]

So far, FORTEC-3D has been applied only for ions, thus test particle collision term does not involve unlike-particle (ion-electron) collision because of the large mass ratio of ion to electron. However, electron NC transport calculations, which are carried out in this paper, require unlike-particle, or electron-ion collision term in addition to like-particle (electron-electron) collision term. Thus a new test particle collision operator is added for FORTEC-3D for electron-ion collisions.

B. Collision operator for unlike-particle

In FORTEC-3D for electrons, ion distribution function is assumed to be a local Maxwellian with average velocity $V_i = 0$, then electron-ion collision term is written as follows:[21]

$$C_{ei} = \frac{\nu_{ei}}{2}L(f_e) = \frac{\nu_{ei}}{2}\frac{\partial}{\partial\lambda}(1-\lambda^2)\frac{\partial\delta f}{\partial\lambda}, \qquad (15)$$

where L represents a Lorentz (pitch angle scattering) operator and λ is the pitch angle of the particle defined as $\lambda \equiv v_\parallel/v$. ν_{ei} is the collision frequency between electron and ion. Since ion is assumed to be a stationary local Maxwellian, only pitch angle collision between electron and ion is

required. In FORTEC-3D pitch angle scattering represented above Eq. (15) is modeled by random change of a particle pitch angle in velocity space as follows:[22]

$$\lambda_n = \lambda_{n-1}(1-\nu_{ei}\tau) \pm [(1-\lambda_{n-1}^2)\nu_{ei}\tau]^{1/2}, \qquad (16)$$

where τ is a simulation time step and subscript n represents a n-th time step in calculation time. It is noted that the sign of the second term in the right hand side in Eq. (16) is randomly determined. Since simulation markers in FORTEC-3D are not monoenergetic but are distributed in the velocity space (initially Maxwellian in the velocity space), some of them have very slow velocities, or large ν_{ei}. This results in the existence of particles which has the collisionality of $\nu_{ei}\tau > 1$. The collision operator above cannot be applied for such particles. The pitch angle for such slow particles at the n-th step is determined by choosing a random number in the $-1 \le \lambda \le 1$ regardless of the pitch angle at the $(n-1)$-th step. In this way, FORTEC-3D for electrons simulate not only the small angle scattering but also the large angle scattering for particles with slow velocities. It is noted that in FORTEC-3D, three constants of motion of total particle number, momentum, and energy are all conserved for like-particle (in this case, electron-electron) collisions with proper field particle operator, while they are not the case for unlike-particle (electron-ion) collisions described in this section, that is, momentum is not conserved for electron-ion collisions.

C. GSRAKE and DCOM/NNW

In this subsection, difference among FORTEC-3D, GSRAKE, and DCOM/NNW is briefly reviewed. Although GSRAKE and DCOM/NNW calculate NC particle and heat flux as well as FORTEC-3D, there are some essential differences in GSRAKE and DCOM/NNW from FORTEC-3D due to the assumptions they adopt.

GSRAKE solves ripple-averaged DK equation for both ripple (helical) trapped particles and transit (passing) ones. It is noticed that the Fourier components of magnetic field B_{mn} with high-n, or $|n| \ge 2$ are neglected in ripple averaging procedure in GSRAKE. In addition to this, GSRAKE assumes that the typical particle's drift velocity is small enough that the deviation of particles from one flux surface during one bounce motion is very small for both trapped and transit (passing) particles, thus the local treatment can be applied: $\Delta r/L \ll 1$ is assumed for plasma particles, where Δr and L the drift orbit width of a particle in the radial direction and the typical scale length such as the density or the temperature gradient. Namely, the particle and heat diffusion due to collisions can be determined only by plasma parameters on a particular magnetic surface. However, such assumptions may be invalid when CERC plasmas are obtained and eITB is formed, since in such plasmas the temperature gradient becomes steep and the temperature itself at the core increases and then the FOW effect may be important even for electrons, though the FOW effect have been considered to be negligible so far. In other words, due to the high T_e in CERC plasma, the collisionality in such plasma becomes low, and then, particles in either the superbanana regime, or the $1/\nu$ regime, can move freely without interruption by any colli-
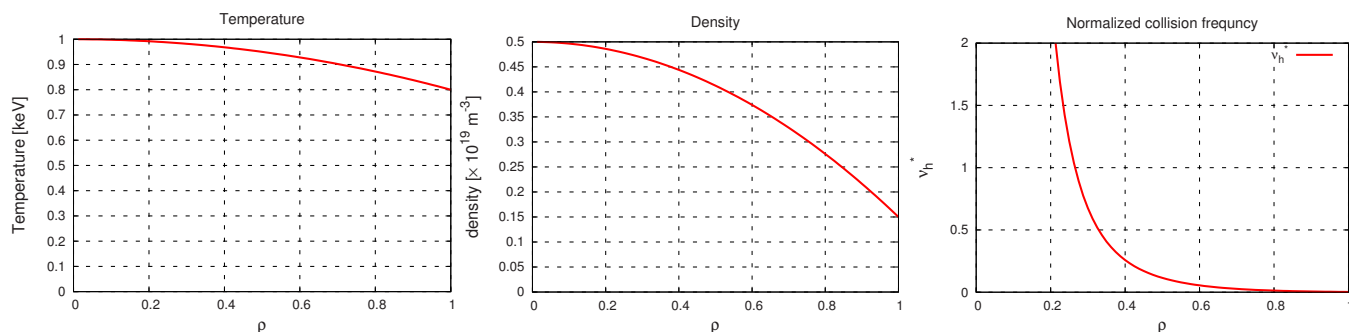
FIG. 1. (Color online) Plasma profile used in the benchmark calculation. The electron temperature (left), density (center), and the resulting collisionality are shown respectively. It is noted that $T_e = T_i$ and $n_e = n_i$ are assumed. Collisionality is shown as normalized value as $\nu_h^* = \nu_{ei}/[\epsilon_h^{3/2}(\nu_{th}/qR)]$, where ϵ_h denotes the helicity of the magnetic field.

sions for a long time, so that the global nature of particle orbits is of great importance to evaluate its NC transport. Finally, GSRAKE adopts only the pitch angle collision term (Lorentz operator). It is noted that although the operator does not satisfy momentum conservation for like-particle collisions, it is shown in Ref. 23 that the precise momentum-conserving collision operator is not so important for the radial transport in the low collisionality regime.

On the other hand, DCOM/NNW calculates NC particle and heat flux based on full DK equation without ripple averaging as well as FORTEC-3D. And there is no limit on magnetic mode number in DCOM/NNW. DCOM/NNW just follows monoenergy particle's trajectory and calculates the diffusion coefficient $D(K)$ from the particle's deviation from a particular magnetic surface after several time steps as,

$$D(\Psi, K) = \frac{1}{2tN}\sum_i^N (\Psi_j(t) - \Psi_{j,0}),\tag{17}$$

where N represents the number of particles, K is the kinetic energy of the particle, $\Psi_j(t)$ is the j-th particle radial position at time t, and $\Psi_{j,0}$ is the initial position of that particle. It is noted that in DCOM/NNW practically energy-dependent diffusion coefficient $D(K)$ is evaluated as a function of normalized collision frequency $\nu_{bn}^* \equiv \nu_{ab}/(\nu/qR)$, namely, $D(\nu_{bn}^*)$ is calculated in DCOM/NNW, where ν_{ab} is the collision frequency between species a and b, and q is the safety factor. K, or particle velocity ν is fixed at very low value, which is typically of the order of mega-electron-volts (MeV) to avoid apparent deviation of a particle from its initial flux surface, through the calculation in DCOM/NNW, and ν_{ab} is given as a numerical variable. This use of ν_{ab} instead of the particle energy K enables DCOM/NNW to evaluate the diffusion coefficient from slow particles of which radial drifts are negligibly small in its δf Monte Carlo method, that is, DCOM/NNW is based on the local NC theory. Then diffusion coefficient $D(\Psi)$ at a particular magnetic surface is given by integrating $D(\Psi, K)$ over energy, and this is implemented by integrating $D(\Psi, \nu_{ab})$ over ν_{ab} in DCOM/NNW. It is also noticed that collision operator used in DCOM/NNW is only pitch angle scattering as well as GSRAKE.

Contrary to these assumptions, in FORTEC-3D, particles' orbits with various energy are directly followed in entire plasma volume, and thus, FOW effects for NC trans-

port can be rigorously taken into account. In addition, exact expression for magnetic field can be used in FORTEC-3D and its collision operator for like-particle collision involves energy scattering term and field particle term which conserves total number of particles, momentum, and energy during a calculation.

III. BENCHMARK CALCULATION FOR ELECTRON NC TRANSPORT

Neoclassical particle and heat flux for electrons are calculated by using extended FORTEC-3D described in the previous section. In order to check the validity of our new FORTEC-3D, benchmark calculations are carried out with other codes, GSRAKE and DCOM/NNW, which have been widely used.

A. Calculation condition

Benchmark calculations are carried out for a moderate temperature ($T_e(0) = 1.0$ keV) plasma. Equilibrium magnetic field configuration of $B(0) = 3.0$ T and $R_{ax} = 3.60$ m is adopted for benchmarking. It is known that the NC transport is reduced as the magnetic axis is shifted inward from standard configuration $R_{ax} = 3.75$ m in LHD (so called σ-optimization).[24] This reduction of NC transport results from the fact that in this σ-optimized LHD configuration, the radial excursion of a particle from a flux surface is suppressed, thus it is considered that LHD $R_{ax} = 3.6$ m configuration has a favorable character for the benchmark calculation. As a result, the nonlocal effect or the deviation from a flux surface which is considered to be small in the conventional NC assumption adopted by such as GSRAKE and DCOM/NNW is relatively not significant in LHD $R_{ax} = 3.6$ m magnetic configuration. Also, since the FOW effect of electron or Δ_h is considered to be negligible in such low temperature plasma, the benchmark calculation would agree among these three codes.

For numerical results obtained by FORTEC-3D, to reduce the calculation noise that results inevitably from Monte Carlo method, 2 048 000 000 of marker particles are used in this calculation. It is noted that sufficient number of marker particles are required to guarantee the results from δf Monte Carlo method to reduce the calculation noise which is pro-
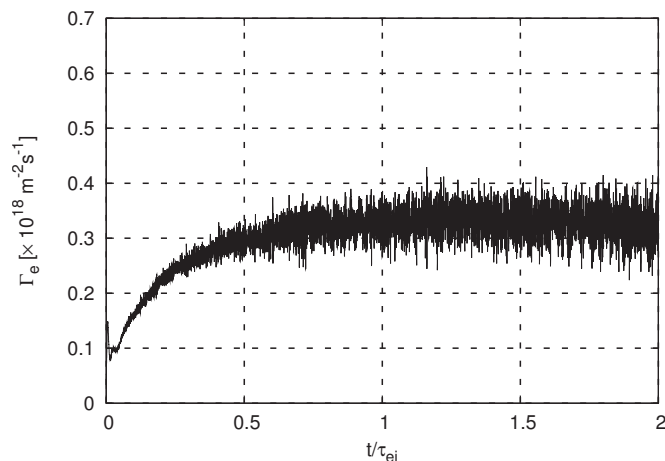
FIG. 2. A typical time evolution of electron particle flux Γ_e by FORTEC-3D simulation is shown.

portional to $1/\sqrt{N}$, where N is the total number of the marker particles. It is also noted that in δf Monte Carlo method, $|\delta f_a/f_{M,a}| \ll 1$ needs to be satisfied in the whole calculation time. In the following calculations, the number of marker particles used here is confirmed to be enough to satisfy $|\delta f_a/f_{M,a}| \ll 1$. It is also noted that a simulation time step Δt is chosen as adequately small to follow a typical marker particle's orbit (e.g., a particle having the thermal velocity) precisely.

Plasma profile used in this calculation is shown in Fig. 1. It is noted that the collision frequency is normalized by the collisionality at the plateau-$1/\nu$ boundary defined as $\nu_h^* = \nu_{ei}/[\epsilon_h^{3/2}(v_{th}/qR)]$, where ϵ_h denotes the helicity in asymmetric magnetic fields. Ion temperature and density are assumed to be same as those of electron for simplicity; $T_e = T_i$ and $n_e = n_i$. The collisionality in this case is in the so-called $1/\nu$ regime for almost the entire plasma. Figure 2 shows a typical time evolution of electron particle flux, Γ_e. The simulation result reaches the steady state in several electron-ion collision times. Energy flux, Q_e, also reaches steady state at the same time in this simulation. In the remainder of this paper, all simulated values of particle and energy flux are averaged over a finite interval in this steady state.

B. Magnetic mode number dependence

As already mentioned in the previous subsection, LHD $R_{ax} = 3.60$ m configuration has a desirable character for the benchmark calculation among those three codes. The magnetic configuration in terms of Fourier components (m, n) for LHD is obtained by using VMEC code,[25] which calculates MHD equilibrium with the given plasma pressure and the current. The equilibrium is converted to Boozer coordinates. Although the magnetic field strength is expressed by many components of B_{mn}, most of them are negligibly small and considered to have no large contribution for the simulation results. Since the number of magnetic field Fourier spectrum used in FORTEC-3D greatly affects the implementation time, numerical results dependence on the number of magnetic mode needs to be investigated to effectively reduce the
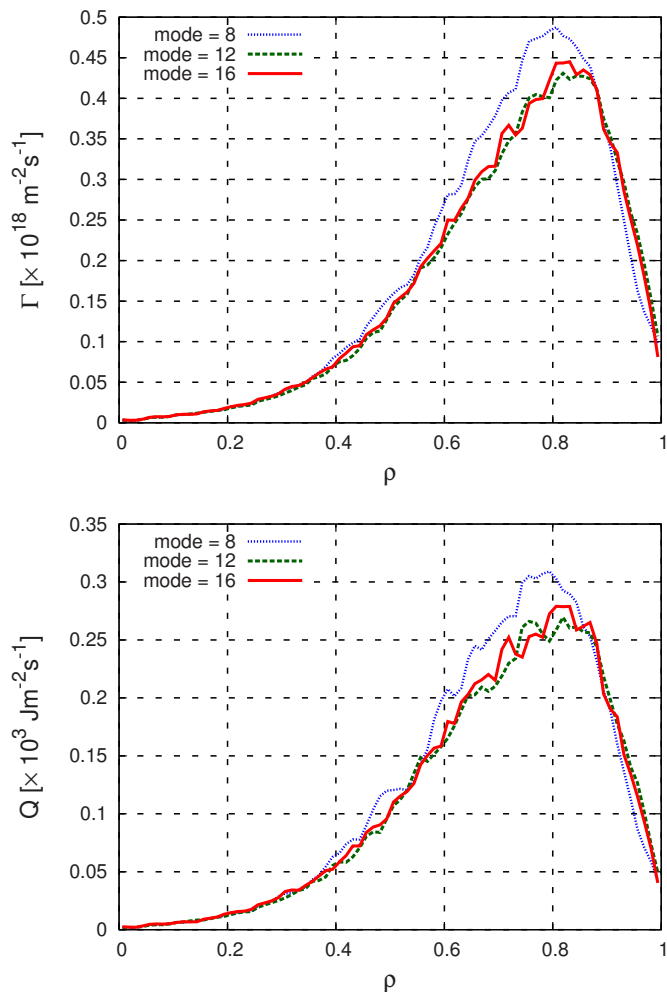

FIG. 3. (Color online) Magnetic field mode number dependence for particle (top) and energy flux (bottom) in FORTEC-3D. For this calculation, $E_r = 0$ is assumed through the entire plasma region.

computational burden. It is noted that the Fourier components used in GSRAKE is 11, namely, $m = 0, 1, 2,$ and 3, and $n = -10, 0,$ and 10 are used.

To check the convergence, three types of calculations for FORTEC-3D are performed for the same plasma parameters with varying the number of Fourier modes, namely, 8, 12, and 16. The results are shown in Fig. 3. It is noted that in this calculation, the same calculation condition (particle number, plasma profiles, etc.) as that mentioned in the previous section are used and $E_r = 0$ kV/m in the entire plasma is adopted for simplicity. In Fig. 3, all the results are averaged over 3000 time steps after reaching steady state. As can be seen clearly in this figure, there is no significant discrepancy when the total mode number $= 12$ or 16 is adopted. Thus, in the remainder of this paper, for LHD $R_{ax} = 3.60$ m magnetic configuration, FORTEC-3D simulations have been carried out with the magnetic mode number $= 12$ or 16. These results show that the truncated higher components of magnetic field affect little the numerical results in FORTEC-3D. When considering the difference of Γ_e between GSRAKE and FORTEC-3D shown in later section, this implies that the
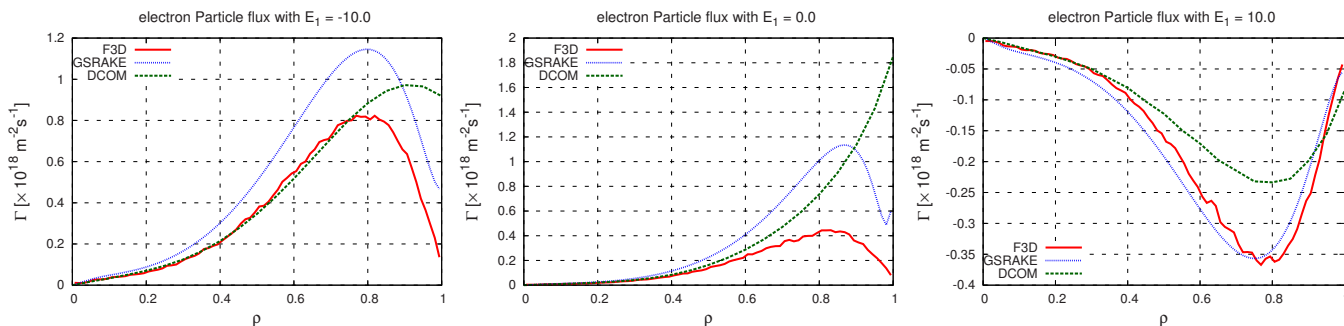
FIG. 4. (Color online) Particle flux calculated by FORTEC-3D (denoted by F3D, solid line), GSRAKE(dashed line), and DCOM/NNW (dotted line) for $E_1 = -10$ (left), 0 (center), and 10 (kV/m) are shown, respectively.

limited mode number used in GSRAKE, which is one of the difference between GSRAKE and FORTEC-3D, does not take much effect on the results.

C. Numerical tests

Based on the discussion above, benchmark calculations have been performed for various E_r profiles to investigate the particle and heat flux dependence on E_r. It is noted that the E_r is given as a radially linear profile for simplicity, that is $E_r(\rho) = E_1\rho$, where E_1 is a calculation constant.

Some of the calculation results are shown in Fig. 4. For each E_r profile, both particle and heat flux reach the steady state as in the previous section and plotted are the values averaged over 3000 time steps. All the cases are calculated by the time $t/\tau_{ei} \simeq 2.0$, where τ_{ei} is a collision time between electron and ion. In this figure, E_r has a linear profile and $E_1 = 10$, 0, and -10 kV/m, respectively. The calculation results obtained by FORTEC-3D are compared with both GSRAKE and DCOM/NNW with corresponding E_r used in

the FORTEC-3D calculation, see Fig. 4. It is clearly shown in these figures that the particle flux calculated by FORTEC-3D has a similar radial profile as that obtained by both GSRAKE and DCOM/NNW for the case of $E_1 = -10$ and 10 cases at the entire plasma region, although its numerical value is different to some extent. Also in the case of $E_1 = 0$, this similarity of radial profile of Γ_e can be seen in Fig. 4 except at the edge region of $\rho > 0.9$. Energy flux is also calculated by these codes and it shows a similar tendency as particle flux.

To see this feature in detail, particle and energy flux dependence on E_r are investigated. In addition to the linear E_r profile used in the calculation above, also the parabolic E_r as $E_r(\rho) = E_1\rho + E_2\rho^2$ is used with varying E_1 and E_2 widely. Particle and energy flux with E_r on $\rho = 0.2$, 0.5 and 0.8 obtained by FORTEC-3D are shown by symbols in Fig. 5. Also plotted are the results calculated by GSRAKE and DCOM/NNW for the benchmarking purpose. It is noticed that at $\rho = 0.8$, both particle and energy flux obtained by
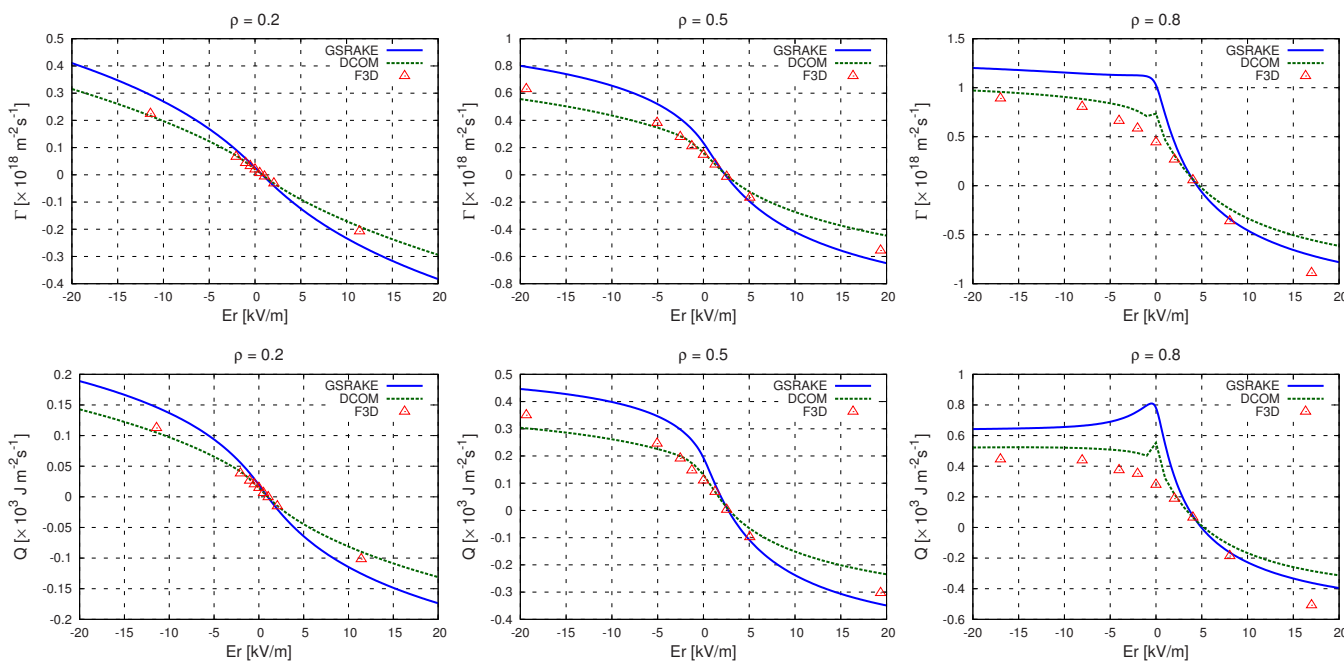

FIG. 5. (Color online) Particle (upper) and energy flux (lower) on various magnetic surfaces ($\rho = 0.2$, 0.5, and 0.8 from left to right) in the benchmark calculation by FORTEC-3D (F3D, symbol), GSRAKE (solid line), and DCOM/NNW (dashed line) are shown as a function of E_r.
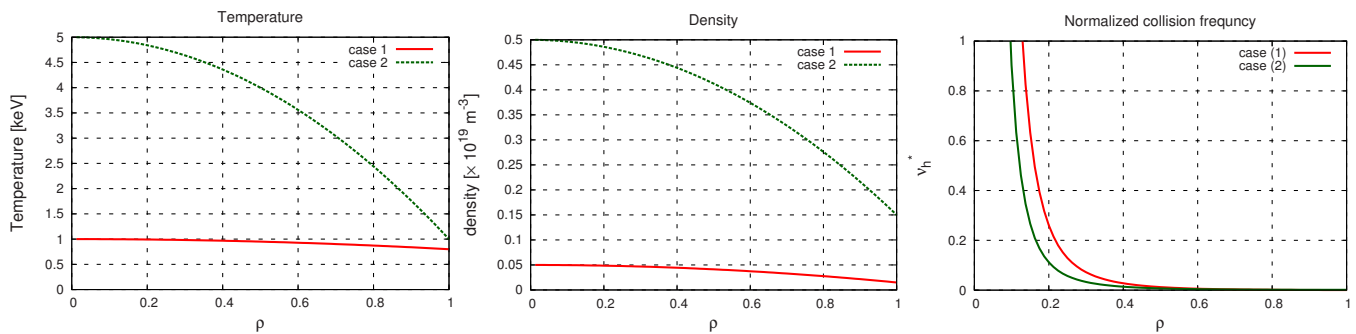
FIG. 6. (Color online) Plasma profile used in the calculation for low collisionality plasmas. $T_e(0)=1.0$ keV and $n_e(0)=0.05\times10^{19}$ m^{-3} for case (1) (solid line) and $T_e(0)=5.0$ keV and $n_e(0)=0.5\times10^{19}$ m^{-3} for case (2) (dashed line) are shown respectively. Temperature (left), density (center), and the collisionality are shown. It is noted that $T_e=T_i$ and $n_e=n_i$ are assumed in these calculations.

GSRAKE and DCOM/NNW codes show a little peaked profile around $E_r=0$, while results from FORTEC-3D are not so. This is the reason why the difference between FORTEC-3D and the other codes increases especially at the outer region for the case of $E_1=0$ in Fig. 4. However, in these figures, it is confirmed that our FORTEC-3D for electrons reproduces the flux curve of E_r dependence obtained by GSRAKE and DCOM/NNW at all surfaces in reasonable accuracy. Consequently, numerical results of FORTEC-3D for electrons show a reasonably good agreement with those obtained by GSRAKE and DCOM/NNW for a plasma with moderate temperature in LHD $R_{ax}=3.60$ m configuration. We can thus conclude that these numerical tests provide a sufficient basis for applying the δf Monte Carlo method to solve the DK equation for electrons involving the nonlocal effect.

IV. CALCULATION RESULTS IN LOW COLLISIONALITY REGIME

Since CERC plasmas in LHD or other helical devices have very high T_e and thus the low collision frequency, precise calculations of NC transport are required to study its confinement property, especially to determine E_r. Thus, particle and heat flux dependence on E_r for plasmas in the low-collisionality regime is investigated. In this section, we perform simulations for two cases of plasmas, that is, FORTEC-3D for electrons has been applied to lower density (case 1) and higher T_e (case 2), respectively. Plasma profiles for these cases are shown in Fig. 6 simultaneously. Also in these figures, normalized collisionality is used as in Fig. 1. These two plasmas are both well in the $1/\nu$ regime as shown in the Fig. 6. It is noted that the calculation in this section are carried out with the total magnetic mode number of 12 in order to reduce computational time since a time step needs to be small enough as in the low-collisionality regime. The values obtained in this simulation are also averaged by 3000 time steps after reaching the steady state. The E_r profiles used for this calculation are similar as used in the previous section, i.e., various linear profiles are adopted. It is noted that the collisionality of each plasma is similar to one another though the temperature and the density are quite different. As discussed in Sec. I, the typical orbit widths of trapped particles, $\Delta_h \propto T_e/\nu_{ei}=n_eT_e^{-5/2}$ for these two cases differ from each other. The radial deviation Δ_h at $\rho=0.5$ is estimated as

$\Delta_h \simeq 0.66$ cm for case (1) and 2.2 cm for case (2) assuming $E_r=0$. Therefore, it is considered that case (1) corresponds to low collisionality case with small radial deviation, while case (2) with large radial drift width. These two cases are both in the low-collisionality regime, so that this radial drift take effect directly on NC transport without E_r. The plasma parameter in case (2) is regarded as a CERC-relevant parameter although T_e has no steep gradient and T_i is higher than that in the typical CERC plasma of $T_i \simeq 1.0$ keV.

The results are shown in Fig. 7 for case (1) and case (2), respectively. The results for case (1) well reproduce the curve of flux dependence on E_r, although the peaked Γ_e profile of GSRAKE and DCOM/NNW around $E_r=0$ make it different from that obtained by FORTEC-3D, especially in plasma outer region (see $\rho=0.8$ case of Fig. 7). This is the similar results as the benchmark test done in the previous section, that is, flux value by GSRAKE and DCOM/NNW has a maximum value with $E_r=0$ in general, while FORTEC-3D shows no such a peak for these low temperature plasmas of $T_e(0)=1.0$ keV. With this simulation, we confirm that our new FORTEC-3D can calculate flux value for less collisional plasma in reasonable agreement with that by GSRAKE and DCOM/NNW except for $E_r=0$. It is noted that in the local NC theory the peaked particle flux at $E_r=0$ reflects the fact that the poloidal resonance occurs when $E\times B$ rotation vanishes. The reduction of the particle flux at the poloidal resonance seen in FORTEC-3D results is discussed later in detail in this section.

When we turn to the results of case (2), however, results from FORTEC-3D make a clear peak around small positive E_r in Fig. 7. One finds that flux calculated by both GSRAKE and DCOM/NNW has a maximum value at $E_r=0$ also in this low-collisionality regime. As a result, this makes qualitatively a significant difference between the evaluated Γ_e by FORTEC-3D and those by the other two codes in the plasma core region, where the CERC plasma has a steep T_e profile. The reason why flux obtained by FORTEC-3D has peaks in positive E_r is that it involves ∇B and curvature drift and takes poloidal resonance effect into account due to the balance between $E\times B$ drift and ∇B and curvature drift. In the local NC theory, the poloidal precession resulting from ∇B and curvature drift is considered to be much smaller than that from $E\times B$ drift, namely $\omega_{E\times B} \gg \omega_B$ is assumed, so that the
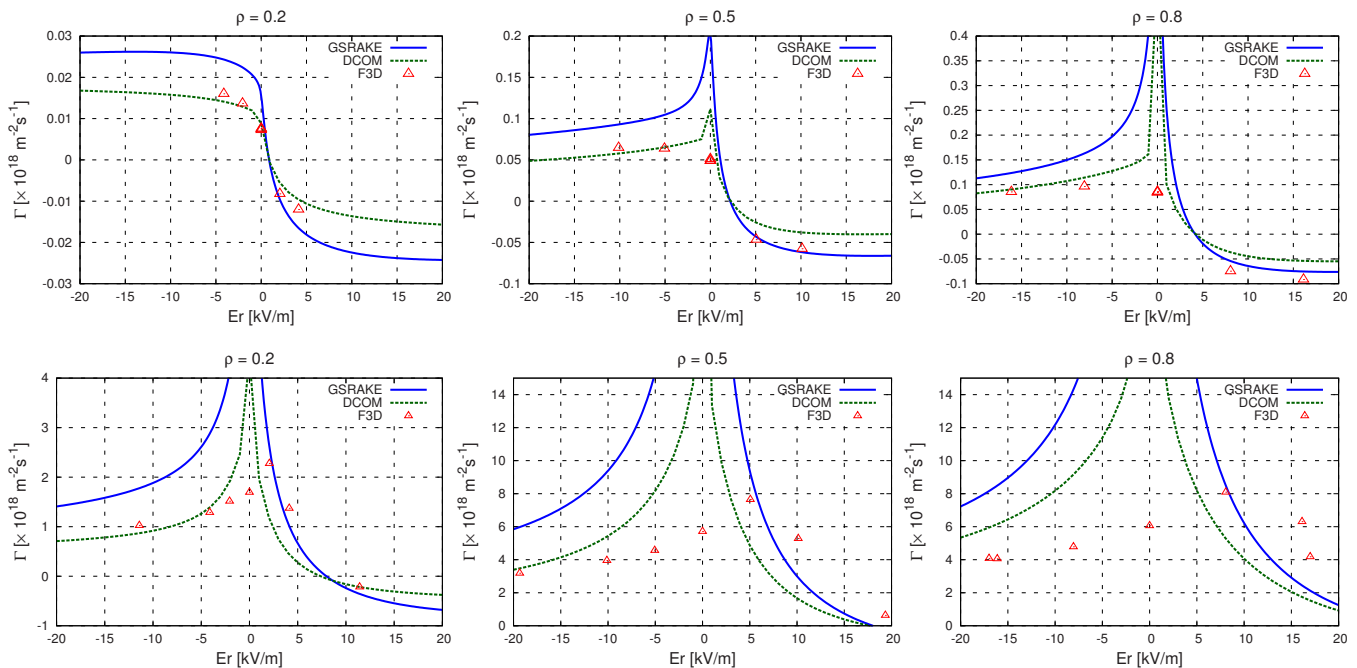
FIG. 7. (Color online) Particle flux on various magnetic surface (ρ=0.2, 0.5, and 0.8 from left to right) for case (1) (upper) and case (2) (lower) calculated by FORTEC-3D (F3D, symbol), GSRAKE (solid line), and DCOM/NNW (dashed line) is shown as a function of E_r.

poloidal motion of particles arises from $\boldsymbol{E} \times \boldsymbol{B}$ drift dominantly, where ω_B denotes the poloidal precession frequency through ∇B and the curvature drifts. It is noted that the ω_B term corresponding to ∇B and the curvature drifts is turned off in GSRAKE calculations in this paper. Also in DCOM/NNW, this effect is not completely taken into account in the calculation since it uses particles of slow velocity. Therefore, the absence of the poloidal component of ∇B and curvature drift which is not included in both GSRAKE and DCOM/NNW leads particle flux obtained by these codes to have a peak at E_r=0 as predicted by the conventional, local NC theory. The ω_B term increases as T_e increases, however, as shown in Fig. 7 case (2) this poloidal precession results in the shifted peak position in the particle flux and needs to be included even for the electron NC transport calculations as is done in FORTEC-3D.

The particle flux obtained by FORTEC-3D shows a clear reduction even when the poloidal resonance occurs as seen in the figures for case (2) in Fig. 7. For case (1), the same results are also seen as the absence of the peaked value of Γ_e for any E_r. It suggests that electrons experience the collisionless detrapping arising from the particle transition from the helically trapped state to passing one due to the FOW effect. This is understood as the following way: in the local NC theory the peaked value of Γ_e at the poloidal resonance follows from the fact that the resonant particles which cause the large NC transport remain in the trapped state as long as the collisional detrapping occurs. If FOW effect exists, however, the helically trapped particle can move radially. The depths of the magnetic field ripple experienced by such particles changes and it leads to the change of the $\partial B / \partial r$ term appearing in the poloidal drift. This results in the break down of the poloidal resonance of particles and causes the collisionless detrapping into passing orbit. It is therefore considered that

the large contribution to the NC transport from the resonant particles, which is predicted in the local NC theory, is reduced by the detrapping due to the radial drift.

In addition to that, NC flux given by FORTEC-3D indicates a relatively small value for all E_r cases at the outer surfaces. This fact indicates that the nonlocal treatment for NC transport without conventional assumptions, which neglect the radial excursion of the particle from the initial magnetic surface, is required even for electrons in order to determine particle flux accurately and then E_r by the ambipolar condition for electron and ion particle flux for high electron temperature plasmas, e.g., CERC.

Consequently, we show that the nonlocal effect of electrons becomes important by the numerical results for the low collisional and high T_e plasmas, where the radial deviation of helical trapped electrons from particular magnetic surface, Δ_h, increases, since this FOW effect along with the poloidal motion of particles can result in a shifted peak in Γ_e at small positive E_r. It is noted that energy flux obtained by FORTEC-3D also shows the same tendency as particle flux, that is, it has a peak around positive E_r not at E_r=0, while that calculated by GSRAKE or DCOM/NNW has a peak at E_r=0. It is concluded that the NC transport for electrons needs to be calculated taking FOW effect into account for high T_e plasmas, since in such plasmas the radial drift of helical trapped particles becomes large so that nonlocality of such particles can contribute to particle and energy flux.

V. SUMMARY AND DISCUSSION

In CERC plasma, the ion temperature remains very low and it would not vary during the plasma discharge as well as ion particle flux, thus it becomes very important to calculate electron particle flux accurately in order to determine E_r and
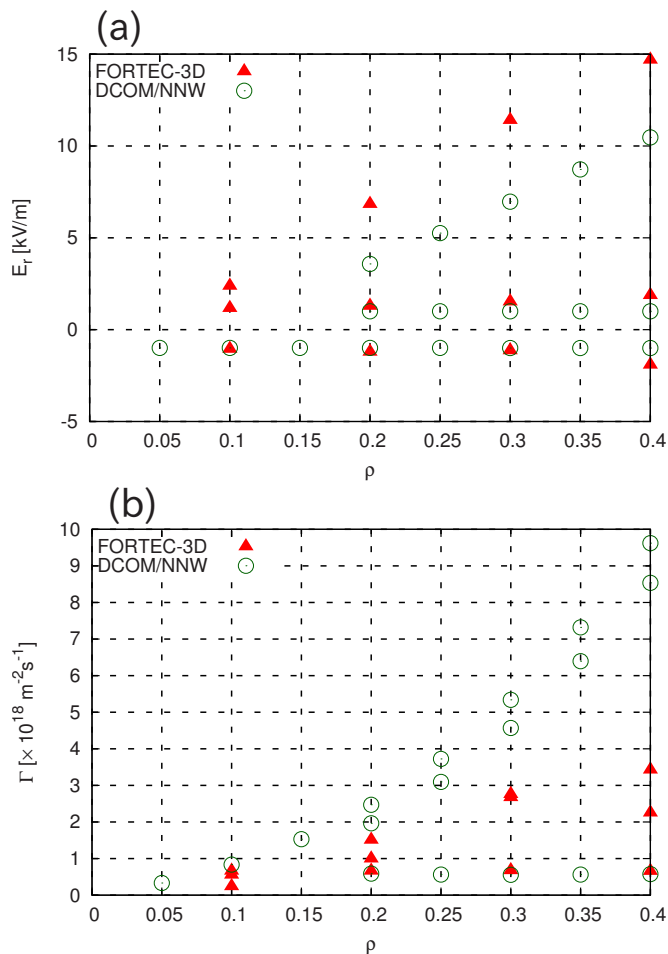
FIG. 8. (Color online) (a) Ambipolar E_r profile obtained from $\Gamma_i^D = \Gamma_e^F$ denoted by FORTEC-3D (red triangles) and $\Gamma_i^D = \Gamma_e^D$ denoted by DCOM/NNW (green circles) are shown respectively. (b) Ambipolar particle flux corresponding to the ambipolar E_r above is shown.

investigate its transition and/or bifurcation phenomenon observed in CERC plasma, since electron particle flux plays an important role in determining whether ion root or electron-root E_r is realized in the plasma. To determine the radial electric field self-consistently in high electron temperature plasmas, which is the motivation of this study, ion particle flux as well as that of electron is required for ambipolar condition. However, simultaneous calculations by FORTEC-3D both for electrons and ions need much computational time, we here roughly estimate the ambipolar E_r and the resultant ambipolar particle flux from the steady-state ambipolar condition of $\Gamma_i^D = \Gamma_e^F$, where superscripts of D and F denotes the particle flux calculated by DCOM/NNW and FORTEC-3D, respectively.

As an example, we take the same plasma used in the previous section of the low collisionality regime {the plasma mentioned by case (2) in the low collisionality calculations], since it has relatively high T_e ($T_e = 5$ keV) at the core and it is considered to be in the CERC-relevant parameter regime. The results are shown in Fig. 8(a) for the ambipolar E_r. It is noted that the values shown by FORTEC-3D is obtained by $\Gamma_i^D = \Gamma_e^F$ while ones by DCOM is obtained by $\Gamma_i^D = \Gamma_e^D$. Multiple values of E_r are seen in this figure and they correspond

to the electron root, unstable root, and ion root from upper one to lower one, respectively. It is also noted that the existence of the electron-root E_r in this region shows the CERC-like character of this plasma parameter. While ion-root and unstable-root E_r is almost the same between E_r by FORTEC-3D and those by DCOM/NNW, electron-root E_r by FORTEC-3D shows larger values than those by DCOM/NNW. In addition, electron-root E_r predicted at $\rho = 0.1$ in FORTEC-3D is not seen from the DCOM/NNW result. It indicates that the resultant ambipolar E_r including electron drift is different from that calculated based on the local NC theory. This results in the significant difference in the evaluation of the ambipolar E_r between local and nonlocal NC transport calculations.

In Fig. 8(b), the ambipolar particle flux is also shown. As in the Fig. 8(a), the multiple values are obtained at some positions and they correspond to the ion-root, unstable-root, and electron-root ones respectively. On the contrary to the ambipolar E_r, ion-root particle flux and unstable-root one show the difference between that by FORTEC-3D and by DCOM/NNW although the ion-root and unstable-root E_r is almost the same for both calculations. Since the ion-root and unstable-root E_r exists in the relatively small $|E_r|$ near $E_r = 0$ compared to electron-root one and Γ_i^D changes sensitively around $E_r = 0$, the resultant ambipolar particle flux corresponding to ion root and unstable root is greatly affected by the slight difference of E_r between that obtained by FORTEC-3D and by DCOM/NNW. On the other hand, electron-root particle flux shows little difference in these calculations despite the difference of electron-root E_r between FORTEC-3D and DCOM/NNW. It reflects the fact that the particle flux does not vary as E_r changes at the larger $|E_r|$ where the electron-root E_r exists so that the electron-root particle flux calculated by FORTEC-3D and DCOM/NNW remains almost the same.

With these estimations above, it suggests that the evaluation of the ambipolar E_r especially for the electron-root E_r requires to take electron drift into account since it expects an electron-root E_r which is not expected by the local NC transport calculation when T_e is sufficiently high. Further application is needed to investigate the electron drift effect on the ambipolar condition and will be performed in the future.

To evaluate electron neoclassical (NC) transport precisely, FORTEC-3D code has been extended to be applicable for electrons. In this new FORTEC-3D code, new collision term involving electron-ion pitch angle scattering is introduced. This enables us to calculate the electron NC particle and energy flux from the drift kinetic (DK) equation without assumptions made in the conventional NC theory and numerical codes, namely, FOW effect for electrons is included in FORTEC-3D.

It is shown that the particle and energy flux calculated by this extended FORTEC-3D for electrons depend not so much on the number of Fourier components of magnetic field of LHD $R_{ax} = 3.6$ m configuration, if 12 or more mode numbers are used. This indicates that higher mode number spectra given by VMEC code have small effect on simulation results since most of those components only have negligibly small value. Afterward, the benchmark calculations have been car-

ried out by using the extended FORTEC-3D code for electrons by comparison with GSRAKE and DCOM/NNW, which both calculate NC particle and energy flux numerically under the assumptions of the local NC theory, which neglect the radial drifts of particles from the initial magnetic surfaces. The results show reasonably a good agreement for a low temperature plasma with $T_e(0)=1.0$ keV for LHD $R_{ax}=3.60$ m magnetic configuration. This calculation condition corresponds to the situation that nonlocal treatment for NC transport is not so important due to the low temperature and the LHD inward-shifted configuration. It is clearly shown in this calculation that flux obtained by FORTEC-3D reproduces that obtained by GSRAKE and DCOM/NNW with various radial electric field on various magnetic surfaces. This provides a sufficient basis that our extended FORTEC-3D can be applied to electrons properly.

Then FORTEC-3D calculations have been performed for low collisional plasmas. For a low collisionality and low temperature plasma, particle flux for E_r by FORTEC-3D again agree well with that obtained by GSRAKE and DCOM/NNW as benchmark test results. With this calculation, we verify the numerical results of FORTEC-3D for electrons in low-collisionality regime. On the other hand, however, for the case of the low collisionality and high temperature plasma, e.g., $T_e=5.0$ keV at the core, the calculation results show significant difference between FORTEC-3D code and the others, especially, for the small E_r cases. Neoclassical particle flux obtained by GSRAKE and DCOM/NNW has a maximum value at $E_r=0$ as in the previous calculations, while peak position of Γ_e from FORTEC-3D moves toward positive E_r. It is considered that this change in the peak profile in E_r is attributed to the effect of poloidal rotation which is determined by the balance between ∇B and the curvature drift and $E \times B$ drift, since this effect is not sufficiently taken into account in GSRAKE and DCOM/NNW. Therefore, we can conclude that the FOW effect and the poloidal motion of particles can result in a definite contribution to NC particle and energy flux in the high T_e plasma, where a large radial drift of a helical trapped particle exists. To evaluate the FOW effect of electrons in more detail, it is required to investigate which types of particles in helical systems contribute to NC flux substantially. It is also suggested that the contribution of the helically trapped particle to the particle flux is prevented due to the particle detrapping processes caused by the radial drift in high T_e plasmas. The detailed analysis for the effect of the particle detrapping on NC transport particle flux also remains the future task. This knowledge may tell us a new way to improve the confinement property furthermore from the point of view of electrons and then the NC ambipolar radial electric field, and it will be done in the future.

In the previous works, FORTEC-3D has calculated only ion particle flux, Γ_i and determined E_r solving its time evolution equation by using E_r-Γ_e table obtained by GSRAKE. Now that FORTEC-3D can be applicable to electrons, we can calculate E_r as the solution of the initial value problem of the ambipolar condition. Whether the ambipolar E_r as obtained in this way is different from that obtained by the local NC theory will be investigated in the practical applications

of FORTEC-3D for the experimental CERC plasmas in the near future. In addition to that, since the balance between electron heat flux and electron heating is considered to be attributed to the formation of eITB, the discrepancies, or shifted peak in energy flux calculation between FORTEC-3D and conventional NC numerical codes is regarded as an important factor to investigate the formation of transport barrier.

ACKNOWLEDGMENTS

[1]H. Takahashi, T. Shimozuma, S. Kubo, I. Yamada, S. Muto, M. Yokoyama, H. Tsuchiya, T. Ido, A. Shimizu, C. Suzuki, K. Ida, S. Matsuoka, S. Satake, K. Narihara, N. Tamura, Y. Yoshimura, H. Igami, H. Kasahara, Y. Tatematsu, T. Mutoh, and T. L. E. Group, IAEA Fusion Energy Conference 2010, Daejon, Korea, 2010, pp. EXC/P8–15.
[2]M. Yokoyama, H. Maaßberg, C. D. Beidler, V. Tribaldos, K. Ida, F. Castejon, T. Estrada, A. Fujisawa, T. Minami, T. Shimozuma, J. Herranz, S. Murakami, and H. Yamada, Fusion Sci. Technol. **50**, 327 (2006).
[3]H. Idei, K. Ida, H. Sanuki, H. Yamada, H. Iguchi, S. Kubo, R. Akiyama, H. Arimoto, M. Fujiwara, M. Hosokawa, K. Matsuoka, S. Morita, K. Nishimura, K. Ohkubo, S. Okamura, S. Sakakibara, C. Takahashi, Y. Takita, K. Tsumori, and I. Yamada, Phys. Rev. Lett. **71**, 2220 (1993).
[4]K. Ida, T. Shimozuma, H. Funaba, K. Narihara, S. Kubo, S. Murakami, A. Wakasa, M. Yokoyama, Y. Takeiri, K. Watanabe, K. Tanaka, M. Yoshinuma, Y. Liang, and N. Ohyabu, Phys. Rev. Lett. **91**, 085003 (2003).
[5]K. Ida, M. Yoshinuma, M. Yokoyama, S. Inagaki, N. Tamura, B. Peterson, T. Morisaki, S. Masuzaki, A. Komori, Y. Nagayama, K. Tanaka, K. Narihara, K. Watanabe, C. Beidler, and LHD Experimental Group, Nucl. Fusion, **45**, 391 (2005).
[6]A. Fujisawa, A. Shimizu, H. Nakano, S. Ohsima, K. Itoh, H. Iguchi, Y. Yoshimura, T. Minami, K. Nagaoka, C. Takahashi, M. Kojima, S. Nishimura, M. Isobe, C. Suzuki, T. Akiyama, Y. Nagashima, K. Ida, K. Toi, T. Ido, S.-I. Itoh, K. Matsuoka, S. Okamura, and P. H. Diamond, Plasma Phys. Controlled Fusion **48**, S205 (2006).
[7]C. D. Beidler and W. D. D'haeseleer, Plasma Phys. Controlled Fusion, **37**, 463 (1995).
[8]C. D. Beidler and H. Maaßberg, Plasma Phys. Controlled Fusion **43**, 1131 (2001).
[9]A. Wakasa, S. Murakami, M. Itagaki, and S.-i. Oikawa, Jpn. J. Appl. Phys. **46**, 1157 (2007).
[10]A. Wakasa, S. Murakami, and S.-i. Oikawa, J. Plasma Fusion Res. **3**, S1030 (2008).
[11]V. Tribaldos and J. Guasp, Plasma Phys. Controlled Fusion **47**, 545 (2005).
[12]K. Miyamoto, *Plasma Physics for Nuclear Fusion* (MIT Press, Cambridge, Massachusetts, 1980).
[13]S. Satake, M. Okamoto, N. Nakajima, H. Sugama, and M. Yokoyama, J. Plasma Fusion Res. **1**, 002 (2006).
[14]S. Satake, R. Kanno, and H. Sugama, J. Plasma Fusion Res. **3**, S1062 (2008).
[15]S. Brunner, E. Valeo, and J. A. Krommes, Phys. Plasmas **6**, 4504 (1999).
[16]W. Wang, N. Nakajima, M. Okamoto, and S. Murakami, J. Plasma Fusion Res. **2**, 250 (1999).
[17]A. H. Boozer, Phys. Fluids **24**, 1999 (1981).
[18]R. G. Littlejohn, J. Plasma Phys. **29**, 111 (1983).

[19] R. B. White, Phys. Fluids B **2**, 845 (1990).

[20] Z. Lin, W. M. Tang, and W. W. Lee, Phys. Plasmas **2**, 2975 (1995).

[21] P. Helander and D. J. Sigmar, *Collisional Transport in Magnetized Plasmas* (Cambridge University Press, Cambridge, UK, 2002).

[22] A. H. Boozer and G. Kuo-Petravic, Phys. Fluids **24**, 851 (1981).

[23] H. Maaßberg, C. D. Beidler, and Y. Turkin, Phys. Plasmas **16**, 072504 (2009).

[24] S. Murakami, A. Wakasa, H. Maaßberg, C. Beidler, H. Yamada, K. Watanabe, and L. E. Group, Nucl. Fusion **42**, L19 (2002).

[25] S. P. Hirshman and O. Betancourt, J. Comput. Phys. **96**, 99 (1991).